RES MILITARIS Social Science Journal

A COMPACT MAGNETO-ELECTRIC DIPOLE ANTENNA FOR S-BAND MIMO THROUGH-WALL RADAR

[1]Dr. K. SUDHAKAR,[2]IMRAN KHAN PATAN

Department Of ECE

St. Johns College of Engineering & Technology, Errakota, Yemmiganur

ABSTRACT

To attain adequate penetration depth, through-wall radar antennas need low operating frequency, compact design, and high gain. This work presents a proposal for an ultra-wideband and low-cost magneto-electric (ME) dipole antenna that operates in the S-band and is designed for through-wall radar applications. A method for reducing the size of a structure is obtained by combining a Minkowski-like fractal ground with a folded shorted patch. This combination increases the route of the surface equivalent current. Furthermore, this configuration may be readily fabricated utilizing a multilayer printed circuit board (PCB) at a little cost. The test findings indicate that the final prototype has an impedance bandwidth of 66.7% throughout the frequency range of 1.7 ~ 3.4 GHz. Additionally, the peak gain within this frequency range is 7.73 dBi. It is worth noting that the prototype maintains a steady radiation pattern across its full frequency band. The antenna has a broad frequency range, a small and efficient structure, a substantial amplification, and an economical price, making it appropriate for challenging applications involving transmission through walls. The antenna's performance is evaluated in comparison to the most advanced existing designs to showcase its significant benefits. Furthermore, it has been smoothly incorporated into a Frequency Modulation Continuous Wave (FMCW) radar system, where it has undergone real-world testing and shown exceptional detection capabilities. The user's text contains the following terms: FMCW system, magneto-electric dipole antenna, MIMO array, tiny antenna, and ultra wide band through-wall radar (TWR).

I. INTRODUCTION

Currently, the promising application potential of through-wall radar sensors has attracted considerable scholarly attention. In the fields of security and disaster rescue, through-wall radar can detect the existence and position of human bodies behind obstacles [1], [2], [3], [4]. Moreover, they can be used for non-contact and non-line-of-sight detection of vital signs (such as heartbeat and breathing) [5], [6], [7], [8]. To acquire multi-dimensional information, most radar sensors necessitate the utilization of multiple-inputmultiple-output (MIMO) antenna arrays [9]. Achieving penetration capability necessitates the radar's operation at low frequencies, while high-resolution performance demands a wide frequency band. In through-wall scenarios, signals weaken significantly after wall penetration, necessitating the antennas with high gain performance. Concurrently, there is a substantial need for the system to be miniaturized, ensuring it remains compact and easily portable for individual use. As the initial stage in radar development, the creation of a miniaturized, ultra-wideband, and high-gain antenna design is critical. Meeting all these requirements simultaneously presents significant challenges in antenna design.

There have been several design attempts to the antenna for through-wall radar. Such as in [10], the Vivaldi antenna is employed, and in [11] a log-periodic antenna is adopted, however both of

which are too large to form into arrays and have limited application scenarios. In [12], the Archimedean spiral antenna array is adopted, however with a strong back radiation, which reduced the radiation energy in the front direction.

Compared to the above designs, magneto-electric (ME) dipole antennas have superior characteristics, such as omnidirectionality, high gain, small size, and ultra-wide band, which have been widely used in various applications, including base station for mobile communications, ultra-wideband systems, and millimeter-wave applications [13], [14], [15], etc. However, the complex manufacturing process and high cost have limited the usage of ME dipole antennas. In recent years, many scholars have proposed enhanced designs to expand the applicability of the ME dipole antennas. In [16], a C-band ME dipole antenna is developed using multilayer printed circuit board (PCB) technology and H-shaped ground structure, which significantly simplifies the machining complexity and improves the antenna performance. In [17] and [18], dielectric loading and folded parallel-wall structures are applied to reduce the profile of antenna, but they have brought difficulty to the manufacturing process.

This study proposes an ME dipole antenna operating in the S-band, designed to meet the comprehensive needs of through-wall radar applications. Our goal is to refine the design for practical engineering production, effectively overcoming the previously mentioned challenges. The main contributions of this work are summarized as follows: 1) We introduce a novel antenna design that diverges from the traditional folded parallel-wall structure. Utilizing short patches and metal vias on a multi-layer FR4 substrate with high permittivity, this design achieves a low-profile and facilitates ease of fabrication. 2) Specifically, we propose a Minkowski-like fractal ground design that substantially lengthens the equivalent current path of the magnetic dipole. This innovation allows fora reduction in antenna size without compromising its operational frequency. 3) Experimental results reveal that the antenna has an impedance bandwidth of 66.7% within the 1.7 to 3.4 GHz frequency range, while also maintaining a stable radiation pattern throughout its bandwidth. Ultimately, this research culminates in the development of an ultra-wideband, miniaturized, cost-effective, and high-gain antenna, optimized for S-band through-wall radar sensors.

II. DESIGN AND SIMULATION OF ANTENNA

A. PRINCIPLE OF ME DIPOLE ANTENNA

A classical magneto-electric (ME) dipole antenna is achievable through a vertically oriented quarter-wave patch connected to a planar dipole, as depicted in Fig. 1(a). The lower resonance frequency is determined by the length of the electric dipole, whereas the higher resonance frequency depends on the length of the magnetic dipole. Employing a bow-tie shaped planar structure enhances the broadband capabilities of the electric dipole, permitting the adjustment of the operational frequency band by altering the lengths of both dipoles. When both electric and magnetic dipoles are excited with equal amplitude and in phase, the resultant radiation pattern resembles a rotationally symmetric heart shape, consistent across both the E and H planes, and effectively minimizes backward radiation, as illustrated in Fig. 1(b). The ME dipole antenna design is noted for its simplicity and ability to support wideband applications. However, its traditional metal structure poses fabrication challenges, is cost-intensive, and has a comparatively high profile.

TABLE 1. Comparison of designed antennas.

Antenna	Bandwidth (GHz)	Gain (dBi)	Dimensions L×W×H(mm³)
Classical ME dipole	1.25	7.78	120×120×30
Antenna 1	1.42	4.4	60×60×14
Antenna 2	1.57	4.68	60×60×11.2
Antenna 3	1.84	4.92	60×40×8

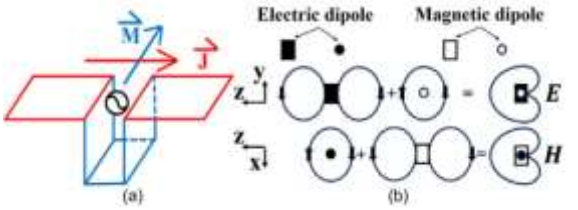

FIGURE 1. Structure of ME dipole antenna, (a) an electric dipole and a quarter-wave patch, (b) principle of radiation pattern formation.

B. MINIATURIZATION DESIGN OF PROPOSED ME DIPOLE ANTENNA

As shown in Fig. 2(a), a classical ME dipole antenna is constructed with center frequency of 2.5GHz. It comprises a large square metal ground, a metal sheet curved by 90 degrees, and an 0−shaped feeding line. The overall height of the antenna is one-fourth of the wavelength corresponding to the center frequency, that is 30mm. The metal structure is quite costly and challenging to fabricate. Recently, the PCB technology has become highly mature and offers easy processing and miniaturization capabilities for PCB antennas, which provides solution to the aforementioned shortcomings of ME antenna.

This study employs an economically viable FR4 substrate to enhance the antenna performance. Fig. 2(b) shows the implementation of antenna 1 of the same bandwidth using a 14mm thick substrate, and the size is greatly reduced with respect to the air since the relative permittivity of the substrate is 4.4. To replace the vertical metal wall of the magneto-electric dipole within the substrate, a series of vertical metal vias are employed. However, due to impractical engineering constraints arising from numerous metal vias and excessive substrate thickness, the structure is divided into seven PCBs each with a 2mm thickness. Next, an antenna 2 is proposed in order to further reduce the profile, as shown

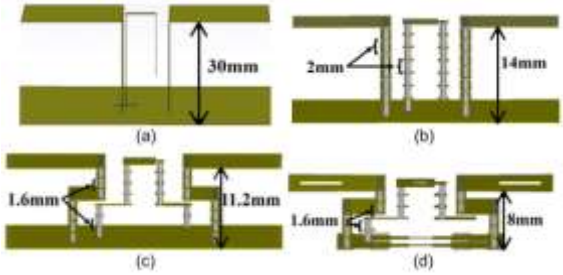

FIGURE 2. (a) Classical ME dipole, (b) antenna 1, (c) antenna 2, (d) antenna 3.

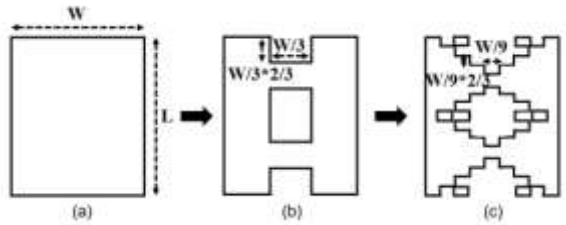

FIGURE 3. (a) 0th-order fractal structure, (b) 1st-order fractal structure, (c) 2nd-order fractal structure.

in Fig. 2(c), where the folded vertical metal wall as in [19] is introduced, and a new folded structure is formed by connecting the printed short-circuit patch with the metal vias of each layer, which reduces the profile by 2.8mm on the basis of antenna 1. At this time, it becomes possible to select a thinner (1.6mm) substrate for regulating impedance matching over a wider range. Considering that it is not easy to assemble antenna 2 with too many layers, we propose a structure of Minkowski-like fractal ground to further reduce the height of the profile and finally realize antenna 3 profile with only 0.067 λ. Compared to previous design, antenna 3 is only divided into five layers each with thickness of 1.6 mm.

The iterative process based on the Minkowski-like fractal proposed in this paper is as shown in Fig. 3, where the rectangular floor is divided into two from the long side, and the length of the rectangular floor is set to be L and the width to be W, and the size ratio of the etched rectangle is set to be 2:3. Small rectangles of

W/3×W/3*2/3 are etched out from each wide side to form the 1st-order fractal structure as shown in Fig. 3(b). On this basis, small rectangles of W/9×W/9*2/3 are etched into the 1st-order fractal structure in the same way to obtain the 2nd-order fractal structure shown in Fig. 3(c). Antenna 3 uses a structure that avoids the coaxial feeding port based on the fractal of 2nd-order. The implementation of Minkowski fractal theory in antenna design significantly enhances the size and bandwidth of the antenna [20], [21], [22], [23] and the Minkowski-like fractal proposed in this paper is innovative on this basis. On the one hand, the Minkowski fractals proposed by the previous literatures are all based on strict square structure, while this paper extends the fractal to arbitrary rectangular

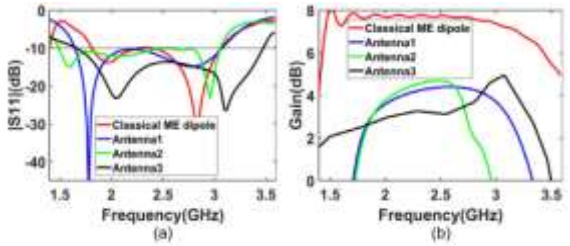

FIGURE 4. Simulation results of the proposed antennas, (a) return loss, (b) gain.

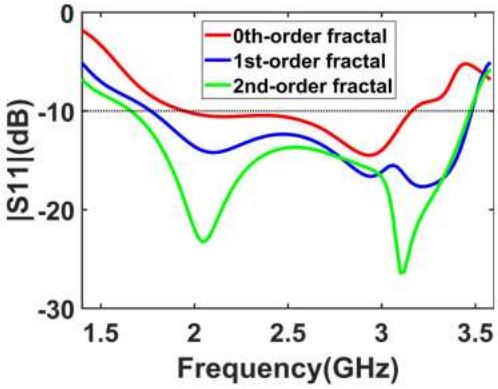

FIGURE 5. Bandwidth at different fractals.

structures. On the other hand, in order to maximize the extension of the current paths, this paper hollows out the middle of the rectangle to realize the fractal in the central part, which doubles the current path as compared to the traditional fractal structures in the literatures.

III. MEASUREMENT AND ANALYSIS

Fig. 6 illustrates the design details of the antenna. The substrate is chosen as FR4 with relative permittivity of 4.4 and thickness of 1.6 mm. Five layers of substrates and reflector are mechanically fastened with plastic screws to form into the antenna with total thickness of 28 mm.

A. ANTENNA GEOMETRY

The top layer is the electric dipole of bow-tie shape, and the square notches are the locations of the plastic screws. The electric dipole operates at quarter wavelength of the medium. Different layers are connected by the vias, located at the inner side of the bow-tie dipole. Two parallel wall structures are created by the vias and the printed short-circuit patches. Excitation of the antenna is achieved by using a 0−shaped probe consisted of a T-shaped patch on the top layer and the vias

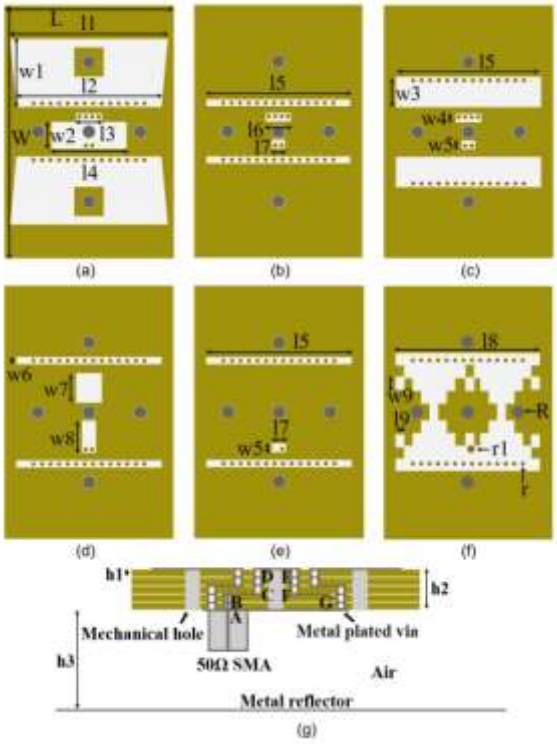

FIGURE 6. Design details of the final proposed antenna, (a) Top layer, (b) second layer, (c) third layer, (d) fourth layer, (e) fifth layer, (f) bottom layer, (g) horizontal cut.

in each layer. The 0−shaped probe, as shown in Fig. 8(g), consists of vertical vias (sections AB,

CD, and EF), printed short-circuit patches (sections BC and FG), and T-shaped patches (section DE). The impedance matching of the antenna is adjusted by the EF and FG sections. The vertical probe is fed by a 50Ω SMA coaxial connector. The SMA internal conductor is inserted into the substrate through section AB, and the external conductor is connected by solder to the Minkowski-like fractal ground. The detailed dimensions of the proposed antenna are as shown in Table 2.

B. RETURN LOSS AND GAIN

Fig. 7 illustrates the |S11| and gain of the antenna, indicating that the measured impedance bandwidth covers a wide bandwidth of 66.7% (1.7 GHz ~3.4 GHz), which is in good agreement with simulation results. The measured in-band gain curve is basically consistent with the simulation trajectory, with a maximum value of 7.73dBi.

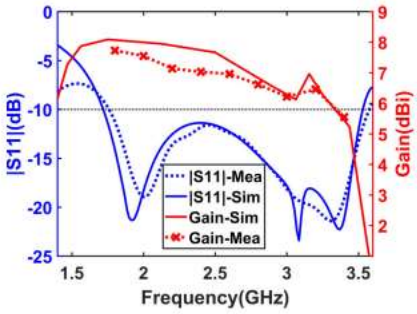

FIGURE 7. Simulated and measured |S11| and gain of the proposed antenna.

C. RADIATION PATTERNS

Three frequency points are selected from the frequency band to analyze the radiation pattern, as illustrated in Fig.8. It is evident that both E-plane and H-plane patterns exhibit a high level of consistency. The measurement data closely aligns with the simulation results. Although the pattern exhibits slight deformation at high frequencies, as evidenced by

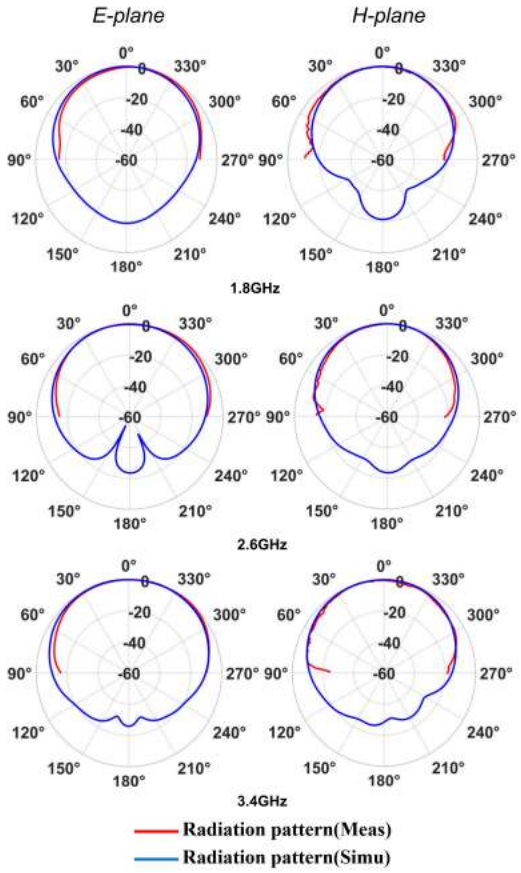

FIGURE 8. Simulated and measured radiation patterns at 1.8, 2.6 and 3.4 GHz.

simulation and measured data, its impact on the system is negligible over a wide range of angles. The actual tested 3dB beamwidth ranges from 70◦ to 91◦ in the H-plane and 81◦ to 105◦ in the E-plane, which can extend the detection range of our radar system and help the radar sensor to recognize targets at large angles.

IV. RADAR SYSTEM AND EXPERIMENTAL SCENARIOS

A. FMCW RADAR SYSTEM

To comprehensively evaluate the performance of the designed antenna, a frequency modulation continuous wave (FMCW) through-wall radar is developed. The whole system is realized by a printed circuit board with dimension 100mm×80mm, and the overall structure of the system is as shown in Fig. 13. The operating frequency band of the radar is 1.8GHz to 3.2GHz while maintaining a transmit power

level of 15dBm. The operating principle of the FMCW system is as indicated in Fig. 14, which depicts the transmitted signal (TX-chirp) and the received signal (RX-chirp) reflected from an object. It should be noted that the RX-chirp is merely a time-delayed version of the TX chirp, where τ represents the round-trip time between the radar and the object, while S denotes the slope of the chirp waveform. The electromagnetic wave reflected by the object is captured by the antenna, amplified and filtered before being fed into the mixer. The output signal of the mixer is the difference between the TX-chirp and the RX- chirp, as shown in Fig. 14(b), which is a signal with a fixed frequency. Then intermediate frequency signal (IF-signal) can be obtained by Fast Fourier

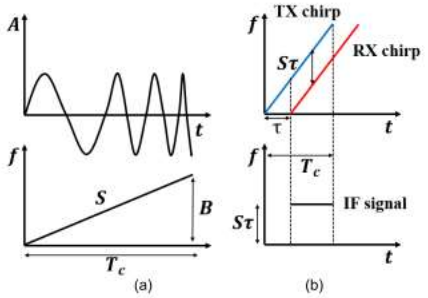

FIGURE 9. Principle of FMCW distance measurement.

Transform (FFT) algorithm after analog-to-digital converter (ADC) acquisition. Finally, utilizing an equation derived below allows us to establish a relationship between IF-signal and distance:

$$c\tau = 2d \quad (1)$$

$$f = S\tau \quad (2)$$

$$f = 2Sd/c \quad (3)$$

where d is the distance from the target to the antenna, and c represents the speed of light.

B. THROUGH-WALL EXPERIMENT

A Vivaldi antenna (since it is mostly used in through wall application) is chosen as comparison to the proposed antenna in through wall experiment. Fig. 15 shows the measured return loss and gain of the Vivaldi antenna. The proposed antenna and Vivaldi antenna are respectively connected to the constructed FMCW radar sensor using 50cm coaxial cable for detecting human targets in complex through wall environments. A subject is involved in the experiment and the consent of this subject has been obtained by a face-to-face interview. The human target walks back and forth for 20 seconds from 2m to 3.5m away from the wall in the house, and the wall is brick and mortar with a thickness of 37cm. A wooden board is placed at 4.5m inside the house to separate the experimental site, with sundries such as cabinets and heaters located behind it. Fig. 16 (a) and (d) show the real scene of the experiment. The distance between the transmitting and receiving antennas is set to 2λ. The Vivaldi antenna is inserted into the foam board to ensure minimal impact on its radiation characteristics, while the antenna proposed in this paper is fixed on the metal reflector. The comparison results obtained by the two kinds of antennas in identical motion scene are presented in Fig.16. The spectrograms correspond to the squared magnitude of the Fast Fourier Transform (FFT) at each frame are presented, with the horizontal axis representing time and the vertical axis representing the distance. The specific value of the spectrogram allows visualizing the strength of the signal reflected from the target over time at different frequencies, where the colormap represents the received echo power. To highlight the target waveform, we truncate the wall reflection interference within 1m in the spectrogram. Slight mismatches are caused by the multiple reflections from other static objects and the multi-path propagation of the wave, since the experiments are conducted in real world situation instead of an ideal environment like anechoic chamber. From Figs. 16 (b), (e), it is evident that the static environment used for the experiment is very complex with multiple strong reflectors. However, Fig. 16 (c) and (f) show that when the human target enters the test field and walks back and forth, a significant triangular

spectrum is generated by the motion which suppresses the interference caused by the static strong reflectors in the environment. The phenomenon has demonstrated the effectiveness of the proposed through wall radar system. From Fig. 16 (c) and (f), one can see that both the proposed antenna and the Vivaldi antenna are able to find the moving human target, while the proposed ME dipole antenna provides significant higher received power spectrum. Obviously, the performance of our proposed ME dipole antenna surpasses that of the Vivaldi antenna, while significantly improves the miniaturization of the whole radar system.

V. CONCLUSION

This research presents a small-sized, highly efficient magneto-electric (ME) dipole antenna that operates in the ultra-wideband frequency range. The antenna is specifically developed for use in S-band through-wall radar applications. It has a maximum gain of 7.73 decibels isotropic (dBi) and an impedance bandwidth of 66.7%. This design preserves the fundamental benefits of ME antennas, such as extensive beam coverage, exceptional performance over a broad range of frequencies, and substantial amplification. Additionally, it accomplishes significant reductions in both manufacturing costs and physical dimensions. A comparison experiment was performed to evaluate the performance of the suggested antenna against the commonly used Vivaldi antenna. The results showed that the proposed antenna not only provides a stronger receiver spectrum but also gives better flexibility for integration into miniature-size MIMO arrays. The suggested antenna has properties that make it very well-suited for MIMO arrays in ultra-wideband, low-frequency radar systems.

REFERENCES

[1] G. W. Kim, S. W. Lee, H. Y. Son, and K. W. Choi, ‘‘A study on 3D human pose estimation using through-wall IR-UWB radar and transformer,’’ IEEE Access, vol. 11, pp. 15082–15095, 2023.

[2] H. Li, G. Cui, S. Guo, L. Kong, and X. Yang, ‘‘Human target detection based on FCN for through-the-wall radar imaging,’’ IEEE Geosci. Remote Sens. Lett., vol. 18, no. 9, pp. 1565–1569, Sep. 2021.

[3] A. Wang, C. Chen, and W. Chen, ‘‘Cluster adaptive matching pursuit for multipolarization through-wall radar imaging,’’ IEEE Sensors J., vol. 23, no. 1, pp. 414–424, Jan. 2023.

[4] Z. Zheng, J. Pan, Z. Ni, C. Shi, S. Ye, and G. Fang, ‘‘Human posture reconstruction for through-the-wall radar imaging using convolutional neural networks,’’ IEEE Geosci. Remote Sens. Lett., vol. 19, pp. 1–5, 2022.

[5] Z. Ling, W. Zhou, Y. Ren, J. Wang, and L. Guo, ‘‘Non-contact heart rate monitoring based on millimeter wave radar,’’ IEEE Access, vol. 10, pp. 74033–74044, 2022.

[6] E. Piuzzi, S. Pisa, P. D’Atanasio, and A. Zambotti, ‘‘Radar cross section measurements of the human body for UWB radar applications,’’ in Proc. IEEE Int. Instrum. Meas. Technol. Conf., May 2012, pp. 1290–1293.

[7] J. Xiong, H. Hong, H. Zhang, N. Wang, H. Chu, and X. Zhu, ‘‘Multitarget respiration detection with adaptive digital beamforming technique based on SIMO radar,’’ IEEE Trans. Microw. Theory Techn., vol. 68, no. 11, pp. 4814–4824, Nov. 2020.

[8] M. Mercuri, I. R. Lorato, Y.-H. Liu, F. Wieringa, C. V. Hoof, and T. Torfs, ‘‘Vital-sign monitoring and spatial tracking of multiple people using a contactless radar-based sensor,’’ Nature Electron., vol. 2, no. 6, pp. 252–262, Jun. 2019.

[9] M. Wang, G. Cui, L. Kong, and X. Yang, ‘‘First-order rear-wall multipath positioning and suppression for through-wall imaging radar,’’ IEEE Sensors J., vol. 18, no. 20, pp. 8261–8274, Oct. 2018.

[10] R. Cicchetti, S. Pisa, E. Piuzzi, E. Pittella, P. D’Atanasio, and O. Testa, ‘‘Numerical and

experimental comparison among a new hybrid FT-music technique and existing algorithms for through-the-wall radar imaging,'' IEEE Trans. Microw. Theory Techn., vol. 69, no. 7, pp. 3372–3387, Jul. 2021.
[11] P.-H. Chen, M. C. Shastry, C.-P. Lai, and R. M. Narayanan, ''A portable real-time digital noise radar system for through-the-wall imaging,'' IEEE Trans. Geosci. Remote Sens., vol. 50, no. 10, pp. 4123–4134, Oct. 2012.
[12] J. Pan, S. Ye, C. Shi, K. Yan, X. Liu, Z. Ni, G. Yang, and G. Fang, ''3D imaging of moving targets for ultra-wideband MIMO through-wall radar system,'' IET Radar, Sonar Navigat., vol. 15, no. 3, pp. 261–273, Mar. 2021.
[13] H. Li, C. Liu, S. Lv, and F. Wu, ''Compact magneto-electric dipole array with wide beam scanning range for 5G NR bands,'' IEEE Access, vol. 11, pp. 88489–88497, 2023.
[14] S. Ni, X. Li, X. Qiao, Q. Wang, and J. Zhang, ''A compact dual-wideband magnetoelectric dipole antenna for 5G millimeter-wave applications,'' IEEE Trans. Antennas Propag., vol. 70, no. 10, pp. 9112–9119, Oct. 2022.
[15] J. Xu, W. Hong, Z. H. Jiang, and H. Zhang, ''Low-cost millimeter-wave circularly polarized planar integrated magneto-electric dipole and its arrays with low-profile feeding structures,'' IEEE Antennas Wireless Propag. Lett., vol. 19, pp. 1400–1404, 2020.